

# A mechanical device to study geometric phases and curvatures

*Accepted for publication in: Am.J. Phys. Jan.2010*

*Salvador Gil*<sup>a</sup>

Escuela de Ciencia y Tecnología, Universidad Nacional de San Martín, Provincia de  
Buenos Aires, Argentina 1653

02.40.Hw, 01.50.My, 01.50.Pa, 01.55.+b, 02.40.Ma,02.40.Yy, 03.65.Vf

A simple mechanical device is introduced that can be used to illustrate the parallel transport of a vector along a curved surface and the geometric phase shift that occurs when a vector is carried along a loop on a curved surface. Its connection with the Foucault pendulum and Berry phases is discussed. The experimental results are in close agreement with the theoretical expectations. The experiment is inexpensive and conceptually easy to understand and perform.

## **I. Introduction**

If a cup is rotated by an angle of  $2\pi$  around a vertical axis, its final state is indistinguishable from the initial state. The same result would be obtained if the cup were transported around a closed loop on the table, keeping the orientation of its handle fixed. In both cases there is no evidence that we have performed these operations. In 1984 Sir Michael Berry made a remarkable discovery<sup>1,2,3</sup> associated with the appearance of a phase factor in the quantum state when a system undergoes a cyclic process.

There are several examples where the wave function acquires a phase factor that is the result of the geometry or topology. For example, there is no magnetic field  $B$  outside a very long solenoid. Nonetheless, if a charged particle loops around the axis of such a solenoid, its wave function acquires a phase that depends on the magnetic flux through the region enclosed by the loop.<sup>4,5</sup> There is also an optical analog of this effect. If linearly polarized laser light is fed into an optical fiber that loops  $n$  times around a cylinder forming

a helix, with the final direction of the beam aligned parallel to the incident direction, the plane of polarization rotates, that is, it experiences a Berry phase shift by an angle proportional to  $n$ .<sup>6</sup>

The failure of certain variables to return to their original values when the system is parallel transported along a closed loop is called *anholonomy*.<sup>1,2,3</sup> This effect is usually associated with the appearance of a phase or a rotation angle (geometric phase shift) that depends only on the topology or geometry of the system. In quantum systems, this phase shift is usually called a Berry phase; its classical analog is referred to as a geometric phase or Hannay angle.<sup>7</sup>

Examples of applications of Berry and geometric phases have been studied in many fields such as quantum field theory,<sup>8</sup> condensed matter physics,<sup>9</sup> atomic physics,<sup>10</sup> and molecular physics.<sup>11</sup> This type of geometric phase shift is also present in several classical systems; the case of the Foucault pendulum is a well known example.<sup>12,13</sup>

Imagine a pendulum in the North Pole; it will oscillate in a plane that seems fixed in space. The same result would be observed if the pendulum were oscillating at the equator, with its plane of oscillation aligned in the east-west direction. At other latitudes, the plane of oscillation will rotate relative to Earth, but slower than at the pole. The period of rotation of the plane of oscillation of a Foucault pendulum at latitude  $\lambda$  is given by  $T(\lambda) = T_{\oplus} / \sin \lambda$ , with  $T_{\oplus} = 23.934$  h (a sidereal day).<sup>13,14</sup> At an intermediate latitude, after a full rotation of the Earth, the orientation of the plane of oscillation of the Foucault pendulum will differ from the initial orientation. This observation reveals the misconception associated with the statement that “the plane of oscillation of the pendulum is fixed in space,” for after  $T_{\oplus}$  the orientation of the Earth with respect to the stars is the same, but the plane of oscillation of the pendulum is not. The angle of rotation of the plane of oscillation after a full rotation of the Earth is the classical analog of the Berry phase shift. This angle depends on the curvature of the Earth through its latitude and retains the history of the process.<sup>12,13</sup>

In this paper we discuss a simple mechanical device that if parallel transported along a curved surface, exhibits a geometric phase effect (anholonomy). This phase or angle gives information about the curvature of the surface along which we have parallel transported the device. Our mechanical device complements a wonderful toy: the Chinese

south-seeking chariot which can be used to study the curvature of surfaces and geometric phases qualitatively.<sup>15</sup>

The experiment is inexpensive and can be done in a basic laboratory setting. The system consists of a frictionless freewheel or flywheel which is restricted to move along a given surface with its axis perpendicular to the surface, that is, the freewheel can rotate with its spokes constrained to the tangent plane of the surface. There is a mark along a spoke of the flywheel as seen in the insert in Fig. 1. The vector defined by the center of the wheel and this mark on the spoke defines the *orientation angle* of the flywheel with respect to a line fixed to the surface. This angle is the only degree of freedom of this device.

In Sec. II we briefly review the concepts of parallel transport and curvature and present a heuristic geometrical model to explain the behavior of our system. This discussion is in the spirit of Refs. 13 and 15, and relates our device to the rotation of the Foucault pendulum. The experimental results are compared to the theoretical expectations in Sec. V. For completeness we summarize in the appendix some basic features of Gauss curvature of a surface and its connection with the phase shift or phase angle that are present in the systems we describe.

## **II. Parallel transport on curved surfaces**

We displace or parallel transport vectors in ordinary space when we need to compare, add, or subtract them. To transport a vector in Euclidean space all that is required is to move the vector, maintaining its magnitude and direction constant (parallel transport). How do we parallel transport a vector in a curved space? This problem was addressed by Levi-Civita<sup>16</sup> who introduced the idea of parallel transport, which was used extensively in the general theory of relativity.<sup>17,18,19</sup> To parallel transport a vector from one point to another on a curved 2D surface, we first connect the two points by a geodesic, that is, a curve that is the shortest distance between two points on this surface. Then we transport the vector along the geodesic, maintaining its magnitude and the angle between the vector and the geodesic constant along the course of the transfer. The same procedure can be applied to parallel transport the vector along a path consisting of several segments of geodesics. On a sphere,

the geodesic corresponds to the segments of a great circle, in particular, the longitudinal lines and the equator are geodesics.

To illustrate the implication of parallel transport along curved space we compare the transport of a vector along a closed loop in flat and curved spaces. On a plane surface the vector remains pointing in the same direction, and therefore its positions at the beginning and at the end of the closed trajectory are indistinguishable. The same phenomenon is observed on a cylindrical surface [Fig. 2(a)]. If a cylinder is cut along any straight line parallel to its axis, it can be opened and laid flat. Because of this property, the cylinder is a surface reducible to a flat surface (see the appendix).

If we parallel transport a vector along a closed loop on a cylinder, the final and initial states coincide. On a spherical surface the situation is different. We begin the trajectory at the pole [point  $A$  in Fig. 2(b)], with the vector tangent to the surface along any longitude and transport the vector parallel to this longitude, maintaining it tangent to this longitude up to the point  $B$  on the equator [see Fig. 2(b)]. Next we parallel transport the vector along the equator up to point  $C$  on a longitude that makes the angle  $\gamma$  with the longitude goes through  $B$ . Finally we close the loop moving the vector along the longitude that goes through  $C$  back to the pole (point  $A$ ). The vector makes an angle  $\delta = \gamma$  with respect to the original orientation.

This phase shift appears whether we transport a vector, an arrow, or a cup. It is a consequence of the curvature of the surface and depends only on its geometrical properties (curvature). If we had a pendulum oscillating at the pole along the longitude  $AB$ , we could similarly transport it along the loop  $ABCA$ . In this case the normal to the plane of oscillation plays the role of the vector. It is clear that the pendulum will show the same type of phase shift.<sup>3,12,13,14</sup>

### **III. Theoretical considerations - Geometrical origin of the phase shift**

If the flywheel of our mechanical device [Fig. 1] moves along a curve on a flat surface, with its axis of rotation always normal to the surface (or flat plane), as indicated in Fig. 2(a), its orientation, defined by a marked spoke, does not change. Similarly, if we parallel transport the flywheel along a great circle on the surface of a sphere, its orientation

does not change. Any great circle on the sphere, that is, a circle generated by its intersection with any plane that includes its center, divides the sphere into two symmetrical halves. From symmetry considerations it is clear that transport along a great circle cannot produce any rotation of the flywheel with respect to the direction defined by the great circle. A rotation of the flywheel in any direction would break the symmetry between the two halves.

We transport the flywheel along the great circles defined by two longitudes separated by the angle  $\gamma$  and the equator (closed trajectory  $ABCD$ ) [see Fig. 2(b)]. If at point  $A$  the vector that defines the orientation of the flywheel is aligned along the longitude that goes through  $B$ , we see that as a consequence of the symmetry property, when the flywheel returns to  $A$  after the cyclic transport ( $ABCA$ ), it will appear rotated by an angle  $\delta = \gamma$ . From Fig. 2 we can see that

$$\frac{2 \text{ area}(ABC)}{4\pi R^2} = \frac{\gamma}{2\pi}, \quad (1)$$

where  $R$  is the radius of the sphere or its radius of curvature. Therefore the phase shift  $\delta$  can also be written as

$$\delta = \gamma = \frac{\text{area}(ABC)}{R^2} = \Omega(ABC), \quad (2)$$

where  $\Omega$  is the solid angle subtended by the area of the spherical triangle defined by the points  $A$ ,  $B$ , and  $C$ . As we will discuss in more detail, the phase angle  $\delta$  can be measured by recording the position of the flywheel with a digital camera or camcorder.

When the flywheel is transported along a parallel of latitude  $\lambda$ , the phase shift can be calculated using the heuristic argument of Refs. 12 and 13. The surface of a cone can be regarded as the locus of all straight line segments joining the apex to the perimeter of the base. The straight line that joins the apex and the perimeter of the base is called the *generator* or *generatrix* of the cone.<sup>22</sup> Imagine a paper cone whose base is parallel to the latitude  $\lambda$  and whose generatrix is tangent to the sphere at this latitude [see Fig. 3]. If the cone is cut along one of its generators, it can be opened out flat without stretching or deformation, and therefore the surface of the cone is also a surface reducible to a flat surface.

The transport of the flywheel around the complete circle of latitude  $\lambda$  produces a phase shift  $\delta$  as indicated in Fig. 3 and can be written as

$$\delta = \frac{2\pi R(\cot \lambda - \cos \lambda)}{R \cot \lambda} = 2\pi(1 - \sin \lambda) = \Omega \text{ (spherical cup)}, \quad (3)$$

where  $\Omega$  represents the solid angle subtended by the spherical cap above the parallel to the latitude  $\lambda$ . This phase shift, expressed in terms of the solid angle, is the same as that of Eq. (2) for the spherical triangle, which is a consequence of the Gauss-Bonnet theorem,<sup>13</sup> a general theorem of differential geometry (see the appendix). This theorem can be used to calculate the phase shift along any closed loop on any type of surface.

Because the addition of a factor of  $2\pi$  to the phase shift is not relevant, we can summarize the result by stating that the transport along a closed loop around a parallel of latitude  $\lambda$  results in a phase shift  $\delta$ , where

$$\delta = -2\pi \sin \lambda = -2\pi \cos \theta, \text{ with } \theta = \pi/2 - \lambda. \quad (4)$$

This result can be used to analyze the Foucault pendulum. In this case it is clear that at the latitude  $\lambda$ , the plane oscillation of the pendulum presents a phase shift  $\delta$  given by Eq. (4) after a full rotation of the Earth. This phase shift changes at a constant rate,

$$|\delta/T_{\oplus}| = 2\pi/T(\lambda), \quad (5)$$

where  $T(\lambda)$  is the period of rotation of the plane of the pendulum at latitude  $\lambda$ . If we combine this relation with Eq. (4), we obtain

$$T(\lambda) = (2\pi/\delta)T_{\oplus} = T_{\oplus}/\sin \lambda, \quad (6)$$

which reproduces period of rotation of the plane of the Foucault pendulum.<sup>12,13</sup> Note that Eq. (6) depends crucially on the shape (curvature) of the Earth. If the Earth were, for example, cylindrical, Eq. (6) would not be valid.

#### IV. The experiment

The experimental setup consists of a low friction flywheel constructed from a commercially available pulley attachment for photogates commonly used in many student laboratories<sup>20</sup> [see insert in Fig. 1]. A copper wire of diameter 2 mm was fixed to the outer edge groove to increase the moment of inertia of the wheel, which is free to rotate around

its axis. The pulley was fixed on a wedge of angle  $\theta$ . The wedge and the flywheel were attached to the plane of a turntable that rotates around a vertical axis [see Fig. 1]. The axis of the flywheel makes an angle  $\theta$  with the axis of the turntable. Note that  $\theta$  is the colatitude equal to the  $90^\circ - \lambda$ ; that is, it is complementary to the latitude  $\lambda$ . A digital camera mounted on a tripod, fixed to the turntable, records the motion of the flywheel and the turntable with respect to a horizontal line drawn on the floor of the laboratory. There are two protractors, one fixed to the floor of the laboratory and a small one fixed to the wedge [seen in the insert of Fig. 1]. The first is used to measure the angle  $\alpha$  between the turntable and a line drawn on the floor of the laboratory. The protractor on the wedge measures the angle  $\beta$  between the flywheel and the wedge fixed to the turntable. A digital camera, operated in video mode at 30 frames per second, allows us to measure the rotation angle  $\beta(t)$  of the flywheel and the angle  $\alpha(t)$  of the turntable as a function of the time  $t$ . For each run of the experiment we chose a wedge that defines the angle  $\theta$ . We turn on the video recording and spin the turntable, first clockwise and then counterclockwise.

## V. Results and discussion

Analyzing the video frame by frame, we obtain for each angle  $\theta$  the angles  $\beta(t)$  and  $\alpha(t)$  as a function of time. Fig. 4 (a) illustrates a typical result. These measurements allow us to plot  $\alpha$  as a function of  $\beta$  as shown in Fig. 4 (b). From the fit of  $\alpha$  versus  $\beta$  the value of the phase shift  $\delta = \beta(\alpha = 360^\circ)$  and its error  $\Delta\delta$  are obtained.

In Fig. 5 we present the results of the phase shift  $\delta$  as a function of  $\theta = \pi/2 - \lambda$ . The error bars in most of the cases are smaller than the symbols. For some angles  $\theta$  we repeated the experiment twice, with results that are in good agreement with each other. At  $\theta = 49^\circ$  we observed a discrepancy between the two runs, but with errors bars that overlap. In Fig. 5 we also indicate by a continuous line the prediction of our model, Eq. (4). The agreement between the experimental results and the theory is excellent.

In comparison to the Foucault pendulum, our mechanical system is low cost and can be used to study the behavior of the system at several latitudes in a single laboratory session. Furthermore, it allows us to explore the changes that take place when the rotation of the turntable changes direction, which would be impossible for the Foucault pendulum.

An interesting challenge is how to modify this device to study other types of surfaces such as a hyperbolic paraboloid, and verify if the results are in agreement with the Gauss-Bonnet theorem.

**Acknowledgments.** This experiment was designed in response to a suggestion by Profs. A. Rojo and D. Garfinkle (Oakland University), who have developed a Lagrangian approach to explain the behavior of the flywheel. Their contribution was essential to the completion of this work and will be published separately by them.<sup>21</sup> The author wishes to thank Dr. A. Schwint, Lic. Hernán Reisin, and Prof. E. Calzetta for a careful reading of the manuscript and valuable suggestions and is grateful to Javier Fernández and Oscar Romanelli for their assistance in building the experimental apparatus. The author also thanks the anonymous reviewers for many valuable suggestions that improved the manuscript.

## Appendix. Brief overview of Gauss curvature and the Gauss-Bonnet theorem

Gaussian curvature is discussed extensively in the differential geometry literature.<sup>19,22,23</sup> In this appendix we summarize some of the results for readers not familiar with this subject. We restrict our discussion to simple connected surfaces (without holes).

Consider a curve described by the function  $y = f(x)$ . Take three neighboring points on the curve and draw a circle through them. The radius of the circle obtained in the limit when the three points approach each other is defined to be the radius of curvature  $R_c$  at that location and is related to the second derivative of  $f(x)$  by<sup>22,23</sup>

$$\frac{1}{R_c} = \frac{d^2 f(x)}{dx^2} \bigg/ \left[ 1 + (df(x)/dx)^2 \right]^{3/2} . \quad (\text{A1})$$

The curvature of the function at that point is defined by  $k_c \equiv 1/R_c$ . It is clear that  $k_c$  and  $R_c$  are local properties of the curve that vary from point to point. The sign of the curvature equals the sign of the second derivative. In particular, for a circle of radius  $a$ ,  $|k_c| = 1/a$ .

Consider a two-dimensional differentiable surface described by  $z=z(x,y)$ . At each point  $p$  on this surface it is possible to define a *normal vector* and a *tangent plane*. Any vector on the tangent plane with origin at  $p$  and the normal vector define a normal plane. The intersection of this normal plane with the surface generates a plane curve, for which it

is possible to define curvature of the type (A1). The curvature varies according to the direction we choose for the tangent vector (orientation of the normal plane). A general result of differential geometry states that for a differentiable surface, there are two orthogonal directions (the principal direction of curvatures) for which the curvatures are maximum ( $k_1(p)$ ) and minimum ( $k_2(p)$ ) respectively.<sup>22,23</sup> The *local Gaussian curvature* of the surface at the point  $p$ ,  $K_G(p)$ , is defined by the product of these two curvatures:

$$K_G(p) = k_1(p) \cdot k_2(p). \quad (\text{A2})$$

For a cylinder or a cone it is easy to see that there is always a direction along which the curvature is zero (along the generatrix). Therefore, for these surfaces the Gaussian curvature defined by Eq. (A2) is zero. These results are consistent with the observation that if we cut a portion of these surfaces surrounded by a simply connected loop, the resulting patch can be laid flat on a plane without tearing or stretching. For a hyperbolic paraboloid (saddle) the curvature along two orthogonal directions has different signs, and therefore the Gaussian curvature for this surface is negative. In contrast, for a sphere the curvatures along any perpendicular direction have the same sign and magnitude. Therefore the Gaussian curvature for a sphere of radius  $a$  is positive and constant:  $K_G=1/a^2$ .

Consider a region  $R$  on a surface enclosed by a loop  $C$  [Fig.6(a)]. The *integral Gaussian curvature* is defined as the surface integral of the local Gaussian curvature:<sup>22,23</sup>

$$IGC = \iint_R K_G dA. \quad (\text{A3})$$

A geometrical interpretation of the integral Gaussian curvature is illustrated in Fig. 6 (Gauss map). At each point along the loop  $C$  we draw a normal unit vector to the surface. Next, we transport each of these vectors to the center of a unit sphere as shown in Fig. 6 (b). As the normal vector on the original surface travels around the boundary  $C$  [Fig. 6 (a)], the corresponding vector in the unit sphere mimics its movement and defines a spherical cap [Fig. 6 (b)]. The area of this spherical cap, equivalent to its solid angle  $\Omega$ , gives the value of the integral Gaussian curvature of the region  $R$  of the original surface enclosed by the loop  $C$ .<sup>22,23</sup>

For a sphere, if we choose the region  $R$  as a spherical cap, limited by a parallel of latitude  $\lambda$  (loop  $C$ ), the original surface and the unit sphere are similar. In this case it is easy to see the equivalence between the two methods for calculating the integral Gaussian

curvature, Eq. (A3), and the geometrical interpretation shown in Fig. 6. Because  $K_G = 1/a^2$ , the integral (A3) is

$$\text{integral Gaussian curvature} = K_G \iint_R dA = \frac{1}{a^2} 2\pi a^2 (1 - \sin \lambda), \quad (\text{A4})$$

which is equal to the solid angle  $\Omega$  that the normal vector maps onto the unit sphere, Eq. (3). Note that the method that Eratosthenes used to measure the curvature of the Earth and the procedure described in Fig. 6 to determine the curvature of a surface are similar.<sup>24</sup>

For a cone of aperture  $\lambda$  [Fig. 7(a)], if the loop  $C$  surrounds the apex, the solid angle of the spherical cap is  $\Omega = 2\pi(1 - \sin \lambda)$ . As discussed in Sec. III, this result is in agreement with Eq. (A4). Similarly, if the loop  $C$  does not contain the apex,  $\Omega = 0$ . These examples illustrate the fact that the curvature of the cone is concentrated in its apex. The concept of integral Gaussian curvature can be extended to any type of surface.

Next consider a triangular pyramid, such as the corner of a cube [see Fig. 8(a)]. While the normal vector travels along the loop  $C$  of one of the (flat) surfaces, the corresponding vector on the sphere remains fixed. When the normal vector turns around the corner at the edge, the vector rotates. When the normal vector completes its journey around  $C$ , the image vector in the unit sphere will have traced an octal on this sphere [Fig. 8(b)], with solid angle  $\Omega = \pi/2$ . The fact that  $\Omega \neq 0$  means that this pyramid has a curvature (although its faces are planes). Again the integral Gaussian curvature of a pyramid is concentrated on its vertex. The cases of the cone and the pyramid illustrate the difference between the local curvature, Eq. (A2), (which is zero in both cases except at the apex, where the local curvature has singularities) and the integral Gaussian curvature, which is nonzero in both cases, as long as the loop encloses the apex. See Refs.22 and 23 for further discussion of this issue.

If the corner of the cube (pyramid) is cut along one of its edges, it can be laid flat on a plane, as illustrated in Fig. 8(c). The borders of the cut make the angle  $\delta = \pi/2$  (missing angle or angle defect) which coincides with  $\Omega$ . Similarly, if the cone is cut along one of its generators, it can be laid flat on a plane with a missing angle  $\delta = \Omega$  [see Fig. 7(c)]. As we will discuss, this amazing property ( $\delta = \Omega$ ) is a consequence of the Gauss-Bonnet theorem.<sup>13,22,23</sup>

On a flat surface the sum of the external angles  $\alpha_i$  of any polygon is equal to  $2\pi$ , as indicated in Fig. 9(a). These results can be interpreted as follows: if we walk along the perimeter of a polygon, after we have completed the journey along the loop, that is, returned to the original point of departure  $A$ , we have rotated around a vertical axis by an angle of  $2\pi$ , which is equal to the sum of the external angles of the polygon. This result is also true if some or all of the corners of the polygon are replaced by smooth curves [Fig. 9(b)]. It is evidently true for a circle or any closed curve on a plane.

The Gauss-Bonnet theorem provides a generalization of this property for a curved surface. On a closed trajectory drawn on a simply connected surface the Gauss-Bonnet theorem states that

$$\sum_i \alpha_i + \text{the integral Gaussian curvature} = 2\pi, \quad (\text{A5})$$

where the integral Gauss curvature is defined by the surface enclosed by the closed trajectory. The sum of the angles  $\alpha_i$  includes all the rotations made along the loop, including those along curved segments. According to our previous discussion, Eq. (A5) can also be written as

$$\sum_i \alpha_i + \Omega = 2\pi. \quad (\text{A6})$$

If we apply this theorem to the spherical triangle  $ABC$  of Fig. 2(b), we have that after we have “walked” around the complete loop, we have rotated around our local vertical axis an angle less than  $2\pi$ , namely, we have rotated, according to the Gauss-Bonnet theorem,  $2\pi - \gamma$ . The missing angle  $\delta = \gamma = \Omega$ , necessary to complete the full  $2\pi$  rotation is the defect angle. This geometrical property is what underlies the anholonomy discussed in Sec. III.

These implications of the Gauss-Bonnet theorem can be illustrated using a spherical piece of fruit (grapefruit) as shown in Fig. 10(a). We cut a narrow strip or spherical segment of the surface along a parallel of latitude  $\lambda$ . This spherical segment cannot be laid down flat on a plane unless we cut it [Fig. 10(b)]. If we do and lay it flat on a plane, the edges of the cut will make an angle  $\delta = \Omega = IGC$ , as illustrated in Fig. 10(c). The resulting anholonomy observed in our mechanical system can be easily visualized. If we parallel transport the flywheel on this flat surface, the orientation of the flywheel will make the angle  $\delta = \Omega$  with the initial longitude, because the orientation of the flywheel remains fixed

in space when we return to the point of departure. Alternatively, if we measure the defect angle  $\delta$  when we parallel transport the flywheel around a loop, we can obtain the integral Gauss curvature of the original surface.

The connection between the defect angle  $\delta$ , the integral Gaussian curvature, and the observed anholonomy in our system is now clear. Our mechanical device, as well as the Chinese south-seeking chariot, provides a direct measurement of the defect angle or phase shift  $\delta$  for the loop on which it travels. From this angle it is possible to infer the integral Gauss curvature of the original surface on which they are transported.

### Figure Captions

Fig. 1: Schematic diagram of the experimental setup. The low friction flywheel is taped on a wedge that constrains its rotation along an inclined axis which makes an angle  $\theta$  with the axis of the turntable. The insert (upper left) is a picture of the flywheel on the protractor which is used to measure its orientation angle  $\beta$  (the angle of the marked spoke measured by the protractor). A digital camera, mounted on a tripod fixed to the turntable, records the orientation angle  $\beta$  of the flywheel and the rotation angle  $\alpha$  between the turntable and a line fixed to the laboratory.

Fig. 2. (a) Parallel transport of a vector or flywheel along the surface of a cylinder. If opened along its generator, it can be laid flat as depicted on the left side of the upper panel. (b) Parallel transport along a sphere.  $\text{Area}(ABC) = (\gamma/2\pi) (1/2) 4\pi R^2$ , and  $\delta = \gamma = \text{Area}(ABC) / R^2$ .

Fig. 3: Parallel transport along a circle of latitude  $\lambda$  on a sphere. When the cone that is constructed around this circle, that is tangent to the sphere along this circle, is opened as indicated on the right, the phase shift of the flywheel is clearly visible.

Fig. 4: (a) The angles  $\alpha$  and  $\beta$  as a function of the time, obtained from the video. (b) The same information, but  $\alpha$  as a function of  $\beta$ . From the fit of  $\alpha$  versus  $\beta$  the value of the phase shift  $\delta = \beta(\alpha = 360^\circ)$  was obtained.

Fig. 5: The phase shift  $\delta = \beta(\alpha = 360^\circ)$  as a function of  $\theta$  (colatitude). The continuous line represents  $\delta = 2\pi \cos(\theta)$ .

Fig. 6: Gauss map which illustrates the geometrical interpretation of the integral Gauss curvature (IGC) of a region  $R$  of a surface enclosed by the loop  $C$ . (a) As the normal vector on the original surface travels around  $C$ , the corresponding vector in the unit sphere defines a (b) spherical cap; its solid angle  $\Omega$  is the integral Gauss curvature.

Fig. 7: (a) Gauss map for a cone of angular aperture  $\lambda$ . (b) The image vector in the unit sphere traces a spherical cap with solid angle  $\Omega = 2\pi(1 - \sin\lambda)$ . (c) The missing or defect angle  $\delta$  is related to  $IGC = \Omega$ .

Fig. 8: (a) Gauss map for a pyramid (cube corner). (b) The image vector in the unit sphere traces an octal on the unit sphere with solid angle  $\Omega = \pi/2$ . (c) The missing angle  $\delta = \pi/2 = \Omega$ .

Fig. 9: (a) The rotation experienced by an observer who walks along the perimeter of a triangle or (b) any closed loop on a plane. If the observer starts at point A, he/she has experienced a rotation of  $2\pi$  along the axis perpendicular to the plane once the journey along the loop is completed.

Fig. 10: (a) The connection between the curvature and the defect angle illustrated with a grapefruit. Two identical spherical segments are cut out of the grapefruit (latitude  $\lambda \approx 50^\circ$ ). (b) The spherical segment cannot be laid down flat on a plane unless we cut it. (c) After the cut, a missing or defect angle  $\delta \approx 90^\circ$  is formed in agreement with  $\delta = \Omega = 2\pi(1 - \sin\lambda)$ .

a) Electronic address: [sgil@unsam.edu.ar](mailto:sgil@unsam.edu.ar)

## References

- 
- <sup>1</sup> M. V. Berry, “Quantum phase factors accompanying adiabatic changes,” Proc. R. Soc. London, Ser. A **392**, 45-57 (1984).
  - <sup>2</sup> M. V. Berry, “Geometric phases in physics,” Sci. Am. **259** (6), 46–52 (1988).
  - <sup>3</sup> M. V. Berry, “Anticipations of the geometric phase,” Phys. Today **43** (12), 34–40 (1990).
  - <sup>4</sup> R. P. Feynman, R. B. Leighton, and M. Sands, *Feynman Lectures on Physics* (Addison-Wesley, Reading, MA, 1970), Vol. 2, Chap. 15.
  - <sup>5</sup> A. Tonomura, N. Osakabe, T. Matsuda, T. Kawasaki, and J. Endo, “Evidence for Aharonov-Bohm effect with magnetic field completely shielded from electron wave,” Phys. Rev. Lett. **56**, 792-795 (1986).
  - <sup>6</sup> A. Tomita and R. Y. Chiao, “Observation of Berry's topological phase by use of an optical fiber,” Phys. Rev. Lett. **57** (8), 937-940 (1986).
  - <sup>7</sup> J. H. Hannay, “Angle variable holonomy in adiabatic excursion of an integrable Hamiltonian,” J. Phys. A **18**, 221–230 (1985).
  - <sup>8</sup> I. J. R. Aitchison, “Berry's topological phase in quantum-mechanics and quantum-field theory,” Phys. Scr. T **23**, 12–20 (1988).
  - <sup>9</sup> P. Ao and D. J. Thouless, “Berry phase and the magnus force for a vortex line in a superconductor,” Phys. Rev. Lett. **70**, 2158–61 (1993).
  - <sup>10</sup> C. Bouchiat, “Cyclic geometrical quantum phases-group-theory derivation and manifestations in atomic physics,” J. de Physique (France) **48**, 1401-1406 (1987).
  - <sup>11</sup> J. Anandan, J. Christian, and K. Wanelik, “Resource Letter GPP-1: Geometric phases in physics,” Am. J. Phys. **65**(3), 180-185 (1997).
  - <sup>12</sup> J. B. Hart, R. E. Miller, and R. L. Mills, “A simple geometric model for visualizing the motion of a Foucault pendulum,” Am. J. Phys. **55**(1), 67–70 (1987).
  - <sup>13</sup> J. von Bergmann and Hsing Chi von Bergmann, “Foucault pendulum through basic geometry,” Am. J. Phys., **75** (10), 888-892 (2007).

- 
- <sup>14</sup> S. T. Thornton and J.B. Marion, *Classical Dynamics of Particles and Systems*, 5th ed. (Brooks/Cole, New York, 2004).
- <sup>15</sup> M. Santander, “The Chinese south-seeking chariot: A simple mechanical device for visualizing curvature and parallel transport,” *Am. J. Phys.* **60** (9), 782-78 (1992).
- <sup>16</sup> T. Levi-Civita, “Nozione di parallelismo su di una variet`a qualunque e conseguente specificazione geometrica della curvatura riemanniana,” *Rend. Circ. Mat. Palermo*, **42**, 173–205 (1917).
- <sup>17</sup> I. R. Kenyon, *General Relativity* (Oxford University Press, London, 1990), Chap.3.
- <sup>18</sup> C. W. Misner, K. S. Thorne, and J. A. Wheeler, *Gravitation* (W. H. Freeman, San Francisco, 1973).
- <sup>19</sup> W. Rindler, *Relativity: Special, General, and Cosmological*, 2nd ed. (Oxford University Press, Oxford, 2006).
- <sup>20</sup> Ultra Pulley from Vernier Software, <[www.vernier.com](http://www.vernier.com)> or Pulley System from Pasco, <[www.pasco.com](http://www.pasco.com)>.
- <sup>21</sup> A.G. Rojo, and D. Garfinkle, “The parallelometer: a mechanical device to study curvature,” *Can. J. Phys.* **87** (6), 615-17 (2009).
- <sup>22</sup> D. J. Struik, *Lectures on Classical Differential Geometry*, 2nd ed. (Dover Publications NY, 1988), Chaps. II and IV.
- <sup>23</sup> A. Gray, *Modern Differential Geometry of Curves and Surfaces with Mathematica*, 2<sup>nd</sup> ed. (CRC Press, Boca Raton, FL, 1997).
- <sup>24</sup> C. Sagan, *Cosmos: A Personal Voyage*, Random House, New York, 1980)

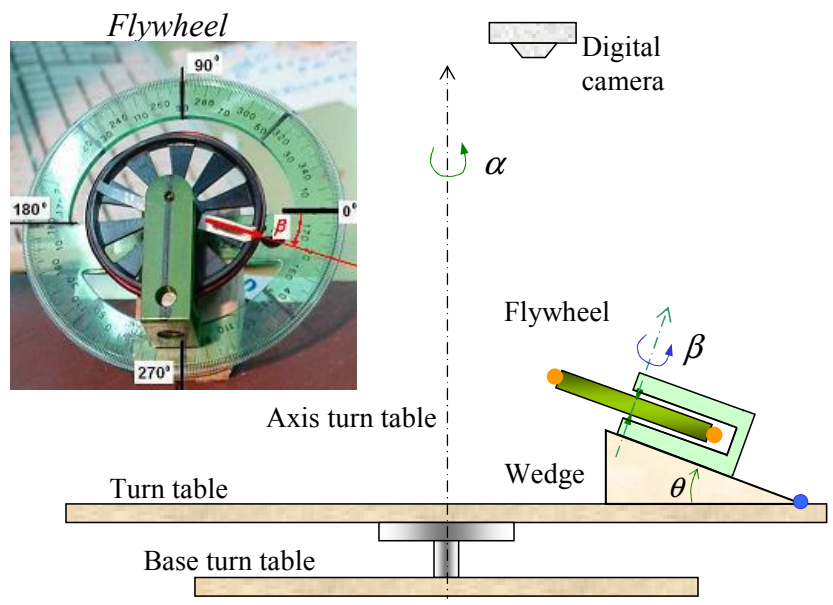


Fig. 1

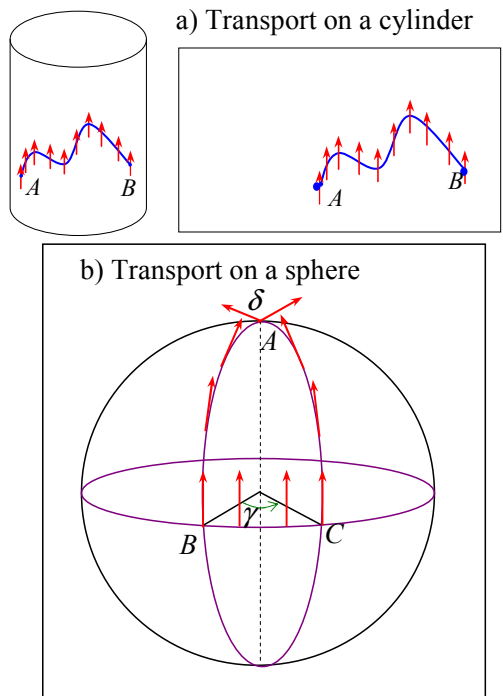


Fig. 2

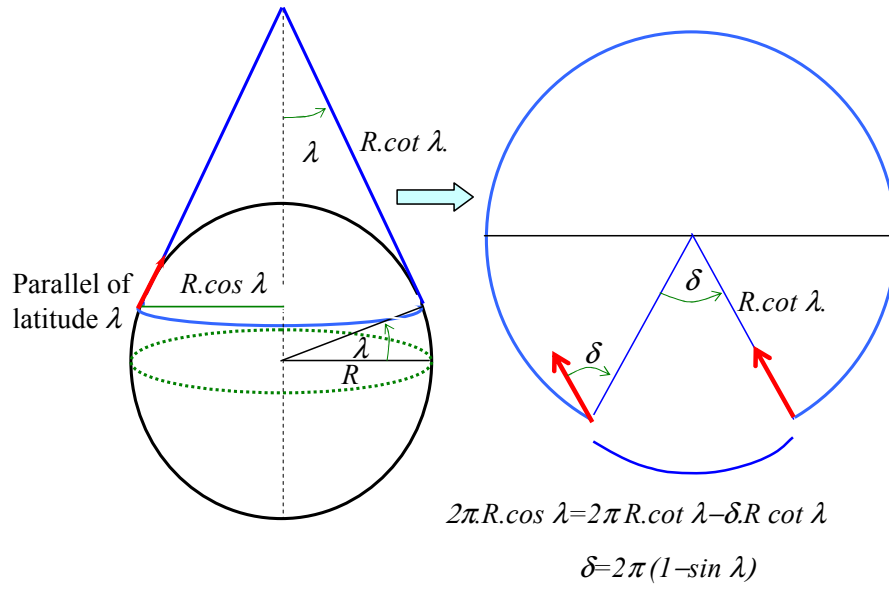


Fig. 3

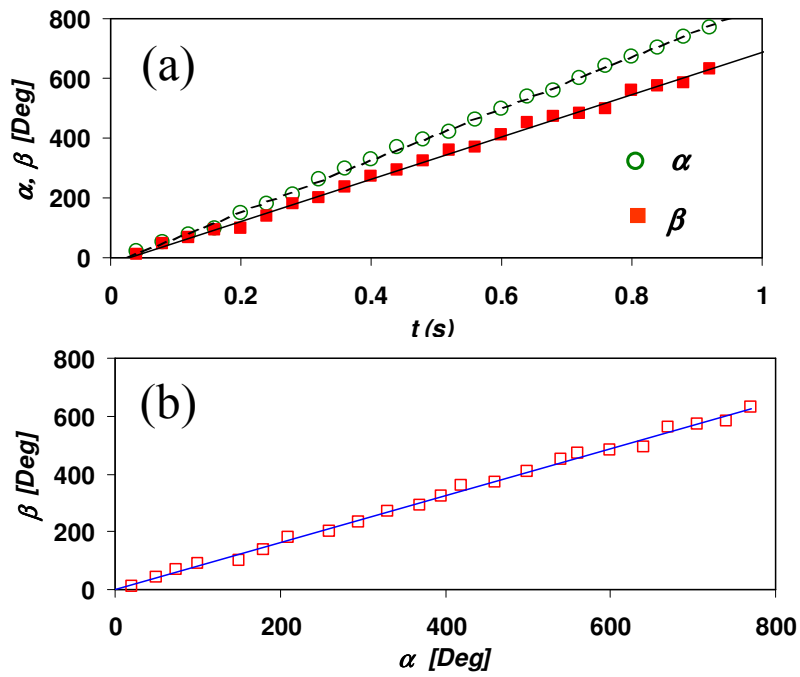


Fig. 4

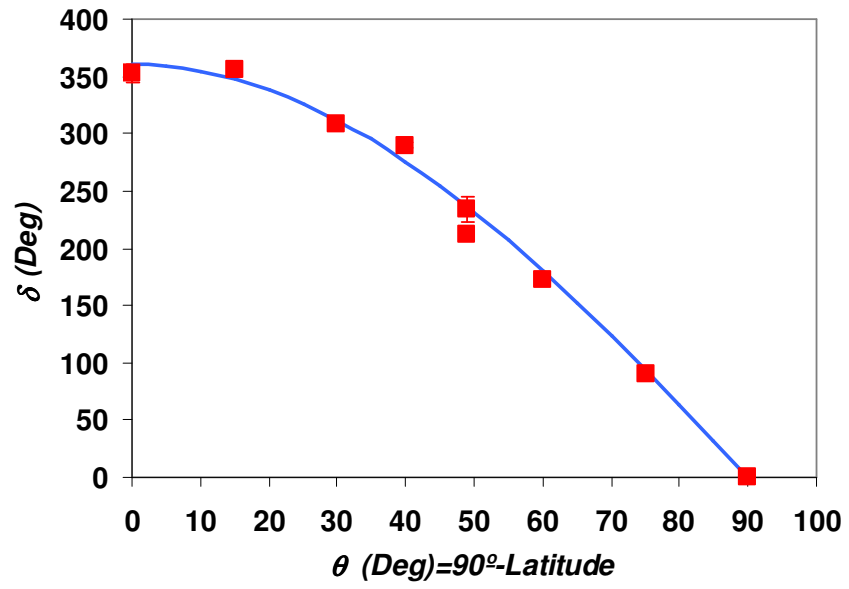


Fig. 5

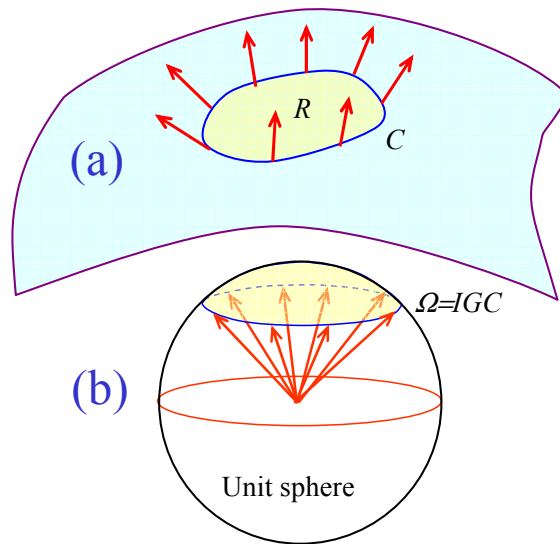


Fig. 6

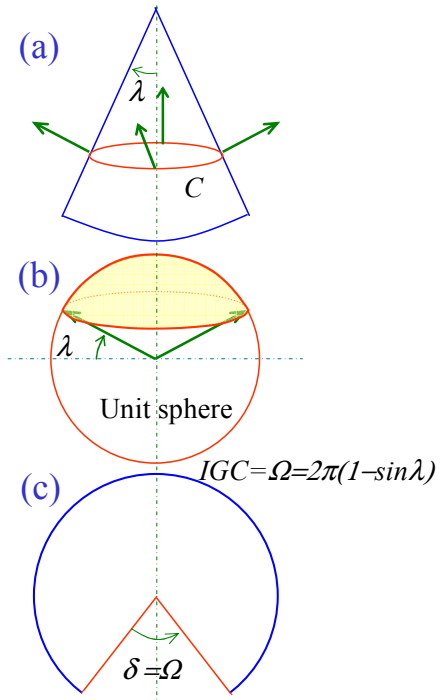


Fig. 7

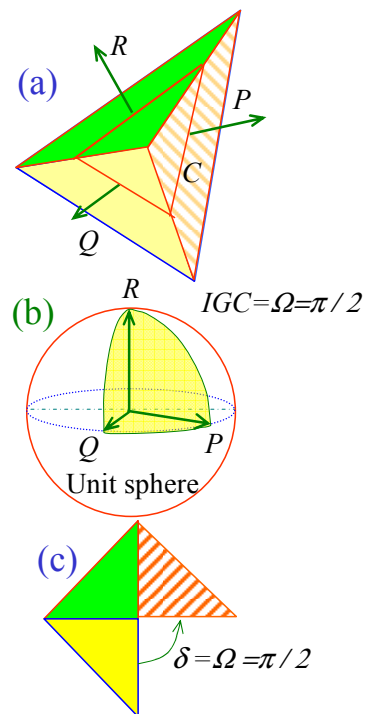


Fig. 8

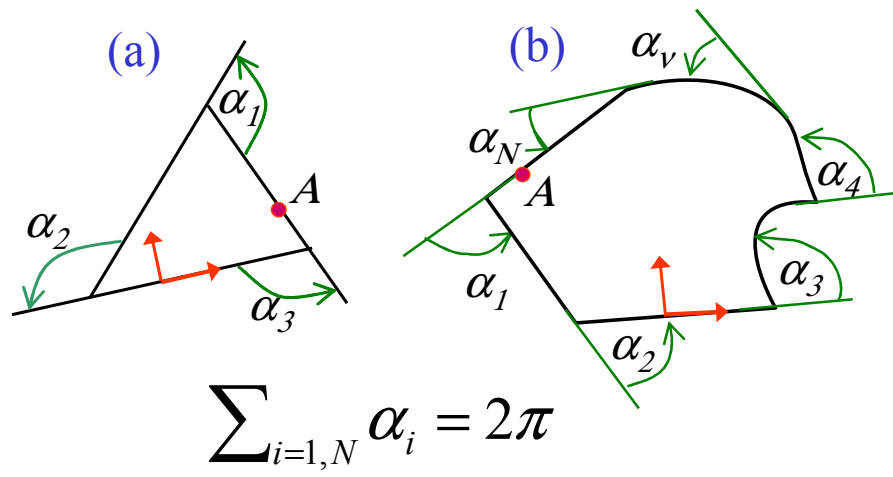


Fig. 9

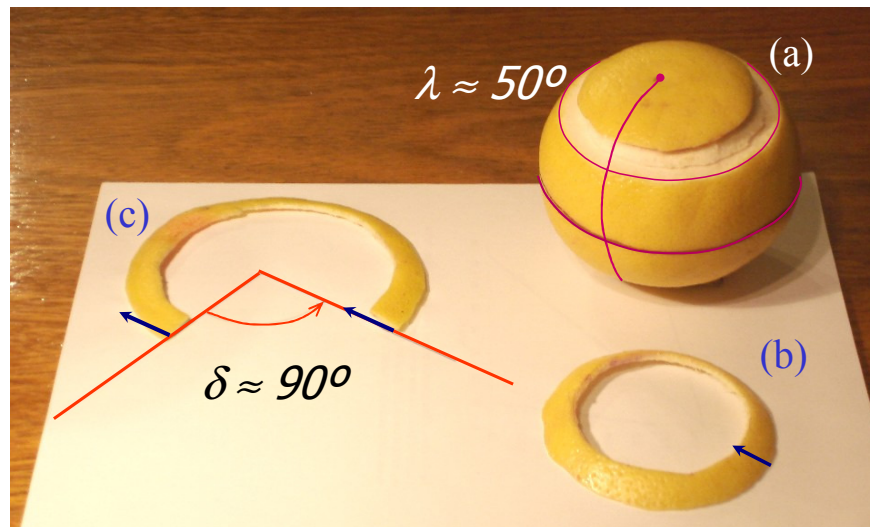


Fig. 10